Elasto-capillary Rolling Transfer Weaves Soft Materials to Spatial Structures

Short title: Elasto-capillary Rolling Transfer

Yue Zhang¹†, Mengtian Yin¹†, Baoxing Xu¹*

¹Department of Mechanical and Aerospace Engineering, University of Virginia, Charlottesville,

VA, USA

†These authors contributed equally

*Corresponding author. Email: bx4c@virginia.edu

Abstract: Spatial structures of soft materials have attracted great attention because of emerging

applications in wearable electronics, biomedical devices, and soft robotics, but there are no facile

technologies available to assemble the soft materials into spatial structures. Here, we report a

mechanical transfer route enabled by the rotational motion of curved substrates relative to the

soft materials on liquid surface. This transfer can weave soft materials into a broad variety of

spatial structures with controllable global weaving chirality and orders and could also produce

local ear-like folds with programmable numbers and distributions. We further prove that multiple

pieces of soft materials in different forms including wire, ribbon and large-area film can be

woven onto curved substrates with various three-dimensional geometry shapes. Application

demonstrations on the woven freestanding spatial structures with on-demand weaving patterns

and orders have been conducted to show the temperature-driven multimodal actuating

functionalities for programmable robotic postures.

Teaser: Elasto-capillary rolling transfer weaves soft materials to spatial structures for

programmable robotic applications

1

Introduction

Spatial structures of soft materials have attracted great interest because, by comparison to conventional planar counterparts, they not only inherit the unique properties of soft materials including low elastic modulus and high mechanical flexibility but also enrich a parameter control space of programing functionalities for a wide range of applications, such as soft robotics (1, 2), wearable electronics (3-6), micromachines (7, 8), microfluidic structures (9) and biomedical devices (10-12). Numerous approaches including direct 3D printing (13-16), and electric (17), magnetic (18), thermal (19), and shape-memory (18)-driven assembly have been developed to fabricate the spatial structures of soft materials over the past years, but usually suffer several practical constraints such as materials ink and printing resolution in 3D printing and intensity and control of exposures in environment stimuli-responsive assembly. As an alternative, mechanical programmable 3D assembly with the support of buckling mechanism is of particular interest because of their good compatibility with well-established planar fabrication processes and has been utilized to design spatial functional structures and devices with a broad variety of geometric morphologies (9, 20-23). Although shape memory materials, buckling modes, and bonding positions between the 2D precursors and pre-stretched soft substrate could be selected and controlled for obtaining desirable 3D structures including free-standing ones for robotic devices (24, 25), transferring the as-fabricated 3D structures onto a specific user set of substrates is challenging. Besides, it relies largely on 2D solid substrates with flat surfaces and requires ultrahigh mechanical stretchability that assists the achievement of large compressive buckling strain for pop-up 3D structures of 2D precursors.

Compared with solid native substrates, liquid phase, an intrinsically mechanical strain-free substrate due to fluidity, could provide a unique and tactful platform that helps release rigid constraints for material fabrication, growth, self-assembly and also avoid residual stress or/and deformation mismatch with solid substrates and is considered an emerging host medium in the preparation of a wide variety of functional materials and devices. For example, liquid-assisted capillary peeling and transfer techniques have been recently developed to produce polymer/CNT based flexible electronics (26), large area 2D materials (27), patterned functional Si membrane (28, 29), and biofilms (30), and the peeling can also help transform the 2D patterns to 3D shapes (31, 32). Liquid evaporation-induced folding and crumpling has also been designed in the assembly of 3D structures (33, 34). These liquid phase-assistant approaches are currently limited

to generating or transferring material patterns and morphologies on a flat substrate and are of critical challenge to produce spatial structures with controllable geometries.

Here, we report an elasto-capillary rolling transfer approach in a liquid substrate surface that enables a fast and facile weave and assembly of soft materials onto 3D curved substrate for spatial structures. The transfer could lead to spatial structures with desirable handedness, weaving orders and arrangements on curved substrates with a broad diversity of geometry shapes including cylinder, sphere and ones with changing curvature for single and multiple forms of soft wire, ribbon and large-area film by controlling rolling direction and orientation and also could produce local structures with ear-like folded shapes by programming transfer directions. Applications on thermal actuation functionalities of freestanding spatial structures composed of thermal conductive soft films have been performed to demonstrate the weaving capability and robustness with well-designed controllability and programmability, potentially useful for mimicking soft and living matters and engineering soft functional devices with spatial structures.

Results

Mechanics and mechanism of rolling transfer for weaving structures

Fig. 1A illustrates the working principle of the elasto-capillary rolling transfer. A cylinder substrate is partially submerged in the liquid bath with a certain depth, and the soft film is positioned onto the liquid surface near the substrate to form an initial contact line among substrate, film and liquid, here referred to as the transfer front, with the direction of α relative to the perpendicular direction to the substrate (x-direction). Upon the sole rolling of the substrate in an either counterclockwise (CCR) or clockwise (CR) direction without translation motion, the film will detach from the liquid and gradually transits onto the substrate across the transfer front, until the entire film is wrapped around the curved surface of substrate. The transferred soft film will form a helical pattern on the substrate with a pitch length Δl .

At the initial state of transfer, the soft film will be mechanically bent at the transfer front by the capillary force (top right schematic of Fig. 1A). With a negligible elongation and local deformation of the soft film at the transfer front (see **Note S1**), our theoretical analysis shows that the transfer front must be above the liquid surface (i.e. h > 0 in Fig. 1A) to allow a pass of film moving upwards for the transfer along the CCR rotation direction; by contrast, the transfer along the CR direction requires the transfer front to be below the liquid surface with h < 0 (**Fig.**

S1A); h = 0 suggests that the capillary force is too small to bend the film, and cannot drive the transfer of film onto the substrate, which can be used to determine the maximum flexural rigidity of film. Particularly, to achieve a successful transfer of mechanically stiff films such as metal films, their thickness needs to be small enough to ensure that the bending stiffness of the films is below the maximum limit. **Fig.** S1B summarizes the effect of the transfer conditions of liquid material phase, rolling velocity and surface wettability of substrate and film, and submerging depth of substrate into liquid on the selection of transfer directions.

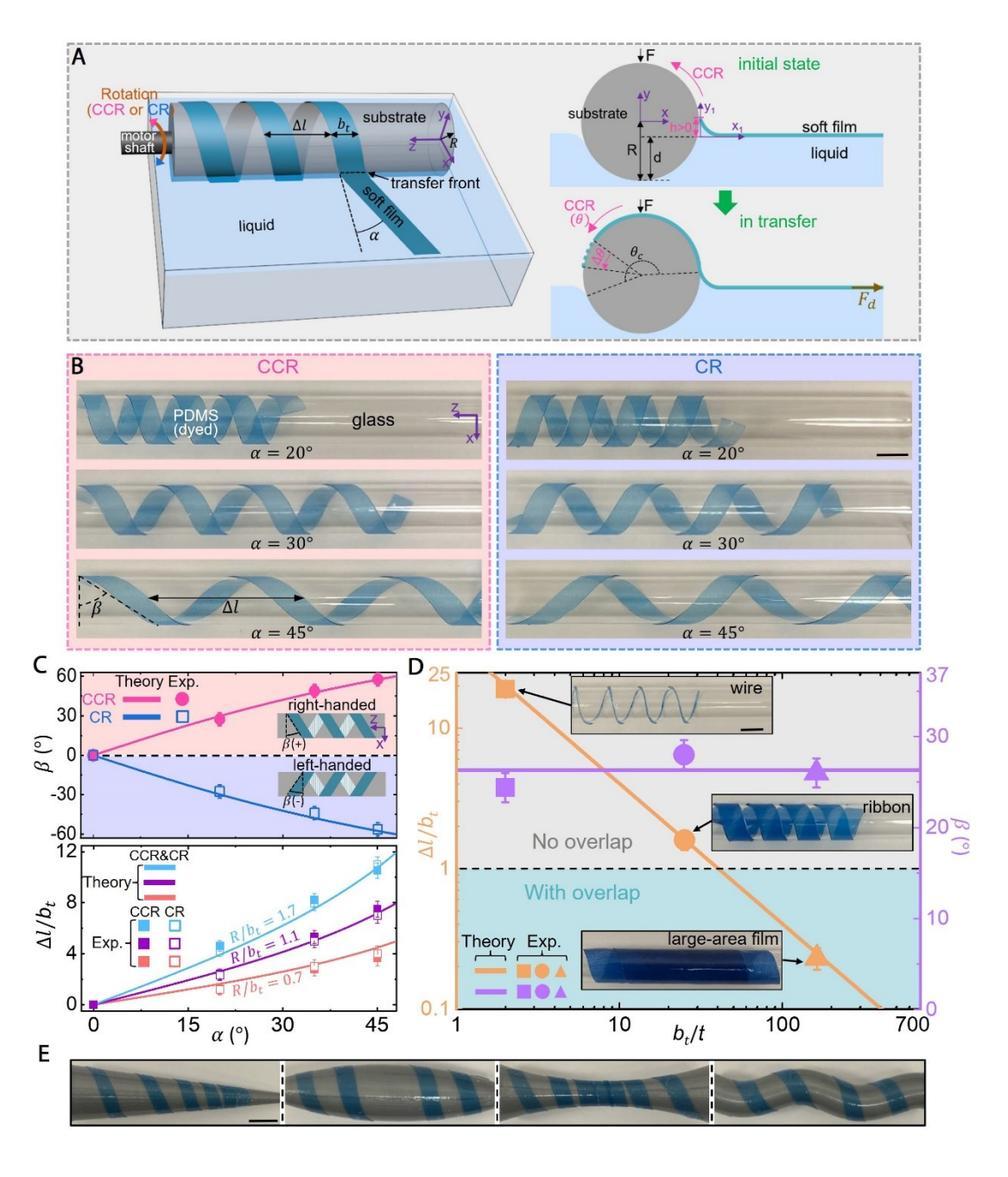


Fig. 1. Elasto-capillary rolling transfer weaves soft film to spatial helical structure on curved substrates. A, Schematic illustrations of the rolling transfer and its working principle. (left) The soft film with width b_t and thickness t was positioned on the liquid surface and contact with 3D substrate at an initial orientation α to form the transfer front. (right) Schematics highlight the transfer front, where the film will be bent at the initial state and the consequent h is the height of transfer front relative to the liquid surface. The counterclockwise (CCR) and clockwise (CR) rotations correspond to h > 0 and h < 0, respectively. After that in transfer, the film will gradually transit onto the rotating substrate across the transfer front. θ is the total rotation angle of substrate with an increment of $\Delta\theta$, and Δl is the pitch of the woven helical pattern on substrate. B, Optical images of the woven spatial helical pattern of soft PDMS film with different rotation direction (CCR or CR) and initial orientation α . In the experiments, the substrate is glass cylinder and liquid bath is water. Scale bar is 1 cm. C, Comparison between theoretical predictions and experimental measurements of the orientation angle β and the normalized pitch $\Delta l/b_t$. $\beta > 0$ for right-handed helical pattern and $\beta < 0$ for the left-handed pattern (insets). D, Weaving feasibility demonstration of soft materials in different geometric forms (wire, ribbon and film) and pattern characterization of the normalized pitch and orientation angle. $\frac{\Delta l}{b_t} < 1$ (cyan area) and $\frac{\Delta l}{b_t} > 1$ (gray area) suggest an overlap and non-overlap in the patterns (insets). The error bars represent the standard deviation from the mean of 10 independent experiments. Scale bar is 1 cm. E, Optical images of the woven spatial structure of soft film on curved substrates with various three-dimensional geometry shapes. Scale bar is 1 cm.

Once the rolling transfer direction of CCR or CR is determined, a successful transfer requires a continuous pass of film across the transfer front (Fig. 1A and Fig. S2) and can also be theoretically predicted by the energy-based model (Note S1). In brief, the transfer process needs to be energy favorable with a decreased total energy with rotation in both transfer directions. In particular, when the viscosity of liquid is low, the mechanical tension energy associated with the stretching deformation of film can be neglected in comparison to its elastic bending energy (Fig. **S3A**). This negligible tensile deformation suggests that no mechanical strain will be introduced to soft materials once transferred onto the substrate by the rolling transfer technique. Besides, a low level of rotation speed of substrate (<1rev/s) will be used in the transfer to avoid the generation of liquid surface wave (35) and obtain a quasi-static stable transfer front. In addition, under a small rotation speed of substrate, our theoretical calculation (Fig. S3B) shows that the energy dissipated due to the viscous drag force can be neglected. Besides, the selection of liquid substrate needs to satisfy a density requirement to ensure that the soft films stay on its surface to minimize the drag force of liquid and remain a stable transfer front during transfer. We should note that the transfer with the rotation angle $\theta \le 360^{\circ}$ (i.e. 1 revolution) is different from that with $\theta > 360^{\circ}$ (i.e. multiple revolutions) for either CCR or CR rolling transfer, and Fig. S4 plots the theoretical phase diagrams of the criterion for a successful transfer of one and multiple revolutions on a wide variety of materials of soft films, transfer substrates and liquid media and controlling parameters of rotation speed and orientation for both transfer directions of CCR and CR. The results indicate the transfer approach can be applied to materials with a broad range of properties and geometries.

Guided by the fundamental working principle and theoretical analysis, we conducted the rolling transfer experiments of a PDMS soft film (slightly dyed for vision, elastic modulus ~2MPa) from a liquid water bath onto a cylinder substrate. With a rotation speed at 1rpm, the film could be continuously transferred onto the substrate in either CCR or CR direction (Fig. S5). In addition, guided by the theory, the initial orientation can be regulated to ensure that a long film can be fully wrapped onto the substrate. Fig. 1B shows a spatial helical pattern of PDMS film on the substrate. With the CCR transfer, the helical pattern has a right-hand handedness, and with the CR transfer, the helical pattern has a left-hand handedness. More importantly, the initial orientation of film α could lead to different pitch Δl and orientation angle β of the transferred helix pattern, which can all be predicted in theory for both CR and CCR transfers (Note S1). Fig. 1C shows that at $\alpha \ge 0$, the orientation angle β is positive and increases with the increasing of α for CCR transfer, and the transferred pattern is right-handed; the β is negative and decreases with the increasing of α for CR transfer, and the transferred pattern is left-handed. Besides, the pitch normalized by width of soft film $\Delta l/b_t$ increases with the increasing of α and substrate radius R. By contrast, the β is independent of the R. More importantly, the experimental measurements (Figs. S6 and S7) agree well with these theoretical calculations. Similar results are also obtained for $\alpha < 0$ (Fig. S8). In addition, at $\alpha = 0$, both the pitch and orientation angle become 0, and the transferred film will be fully overlapped at the same position on substrate for both CCR and CR transfer, as shown in Fig. S6.

Fig. 1D shows that the normalized pitch decreases with the increasing of b_t/t with remarkable consistency with theoretical predictions, where b_t and t are width and thickness of film, respectively. At $\frac{\Delta l}{b_t} < 1$, the transferred pattern shows an overlap; and vice visa. Especially, at $\frac{b_t}{t} \approx 1$, the soft film becomes a wire, and at $\frac{b_t}{t} > 100$, the soft film can be considered a large-area film, indicating that this rolling transfer technique can be used to transfer soft materials with a broad variety of geometric shapes into desired patterns precisely in a well-controlled manner.

Similar to that of Fig. 1C, the β of transferred patterns is independent of the geometry shapes of soft materials and the thickness (i.e. $\frac{b_t}{t}$) even down to a few micrometers (**Fig. S9**). In addition, a series of successful transfer experiments of soft films onto 3D substrates with a diversity of geometry including cone, sphere and saddle shapes confirm the robustness of this rolling transfer technique for potential complex spatial structures, as shown in **Fig. 1E** and **Fig. S10**. It should be noted that for transferring a large-area wide film onto a non-developable substrate counterpart, the films need to be carefully optimized in dimensions to achieve a conformal contact after transfer (36, 37). The optimization design via structural meshing or network design (38, 39) will help introduce extra degrees of freedom on films and relieve the geometric mismatch induced strain after transfer, and the basic size of each piece of optimized film elements could also be similar to the film dimensions that we demonstrated.

Weaving structures with local controllable folded features

Different from a continuous unidirectional rotation for weaving structures of soft film with uniform spatial chirality, when the rotation direction switches during transfer, ear-like folded features can be achieved in the woven structures, as illustrated in **Fig. 2A**. Similar to that of weaving global spatial structures on the substrates in Fig. 1, the formation of these local morphologies is also an energy favorable process, and can be predicted in theory (**Note S2**). **Figs. S11** and **S12** plot the theoretical predictions of minimum rotation angle θ required for successful folding and the radius of formed fold r_{fold} for both dry air and liquid conditions, and they both agree well with experiment measurements from **Fig. S13**.

Fig. 2B shows the optical images (side view) of the transferred PDMS patterns with local folds. When the number of rolling direction switch N_{switch} increases from 1 to 4 during transfer, the corresponding number of folds n will increase from 1 to 4 (Fig. 2B a), in good agreement with the theoretical analysis (Fig. S14). When multiple folds are formed, they could be concentrated in a certain region with a very non-uniform distribution (Fig. 2B b). Particularly, they could be embedded into the spatial layers of the woven structures (Fig. 2B c). The location and dimensional size of these folds can be well controlled by controlling the transfer direction and order and interval of switch (Figs. S15-S18). Fig. 2C shows the schematic illustration of woven structures with n local folds formed at $\alpha = 0$, where the folds are only located in angular (θ) direction. Both the location and size of folds can be predicted in theory (Note S2 and Fig.

S14), and agree very well with experimental measurements for different N_{switch} and transfer directions, as shown in Fig. 2C.

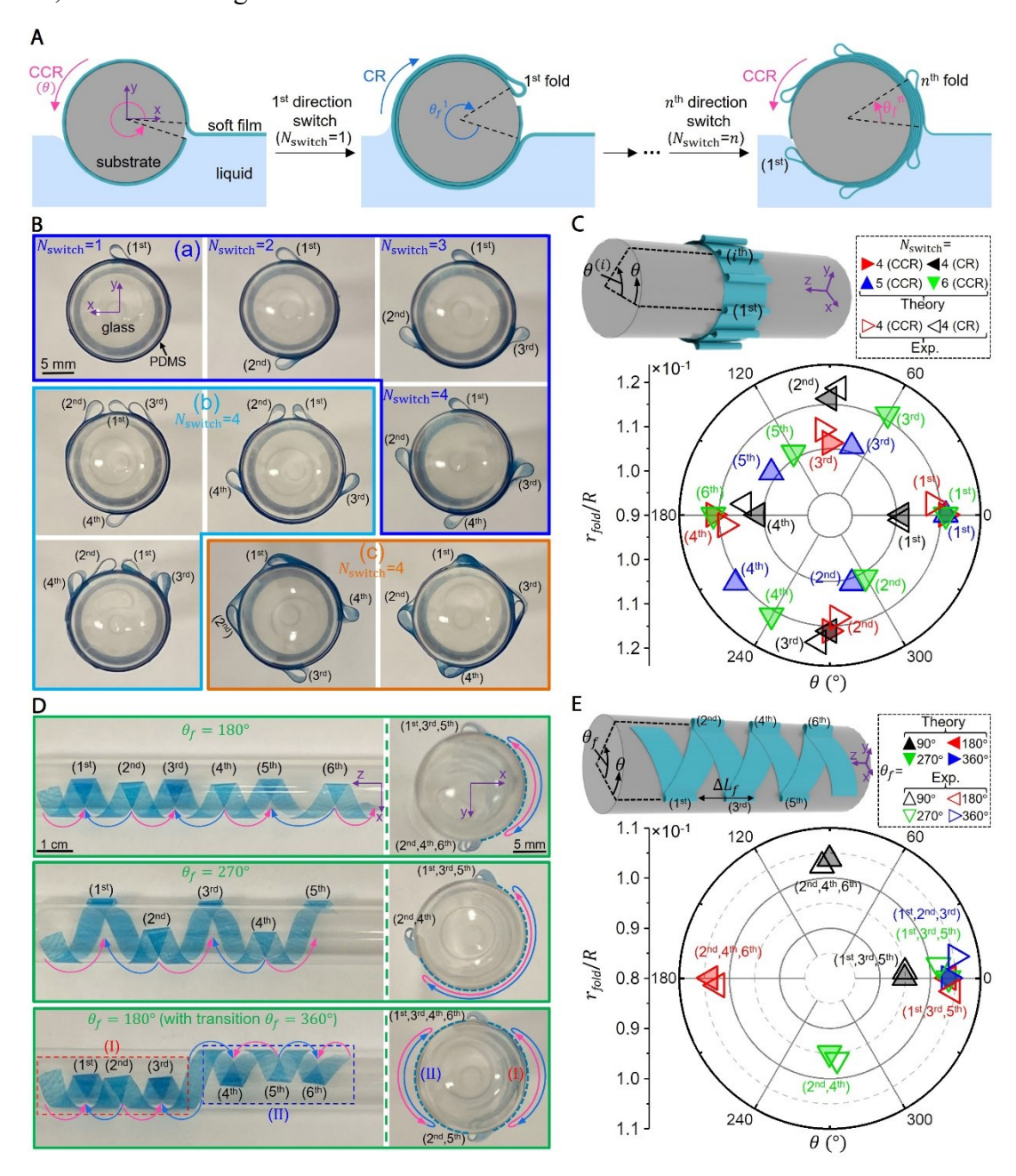


Fig. 2. Weaving spatial structures with controllable ear-like local folded features by transfer. A, Schematic illustration of generating local ear-like folds through the switch of rotation direction with angle θ_f in transfer. The total number of folds n equals to the number of direction switch N_{switch} and the i^{th} ($1 \le i \le n$) fold is formed in the i^{th} direction switch. B, Optical images of the transferred PDMS patterns with local folds obtained by transfer at $\alpha = 0$. The category a shows the patterns obtained with different N_{switch} . The number in the bracket denotes the i^{th} fold formed in the i^{th} direction switch. The category b shows the patterns with 4 folds ($N_{switch} = 4$) in a non-uniform distribution. The category c shows the patterns with 4 folds

embedded into the different spatial layers. C, Location and size of local folds in the woven structures by the transfer at $\alpha=0$, where the location of the i^{th} fold is described by $\theta^{(i)}$ with $\theta^{(1)}=0$. The polar plot (bottom) gives the theoretical predictions and experimental measurements for the radius of fold normalized by the substrate radius r_{fold}/R and the angular location of uniformly distributed folds. D, Optical images of the soft film woven in both axial and angular direction for different periodic rotation angle θ_f at $\alpha=20^\circ$. The position of film in the side view images is highlighted by the blue dash curve. The pink and blue arrows represent CCR and CR rotations respectively. E, Location and size of the folds in the transferred pattern by the transfer at $\alpha>0$. The schematic (top) illustrates that the angular (θ) spacing of folds equals to the rotation angle θ_f , and ΔL_f is the axial (z) spacing of folds. The polar plot (bottom) gives the theoretical predictions and experimental measurements for the normalized radius and angular location of folds.

When the initial orientation of film α is set to non-zero in the transfer, the fold could also be formed along the axial (z-) direction of the substrate, allowing to weave soft films onto a certain partial region of substrate, as illustrated in Fig. S19. With rolling transfer in CCR direction, $\alpha = 20^{\circ}$, and periodic switch angle θ_f , Fig. 2D and Fig. S20 show the optical images of uniformly woven PDMS film on the cylinder substrate in both axial direction (front (x-z plane) view) and angular direction (side (x-y plane) view). When the switch angle changes during the transfer, e.g. increases from 90° to 360°, the resultant woven pattern will also change, covering an increased angular area of the substrate from 90° to 360. Due to its periodicity, the folds are formed in symmetry on the spatial cylinder substrate with angular spacing equal to θ_f , as shown in the schematic of Fig. 2E. Similar to that of folds at $\alpha = 0$ in Fig. 2C, the total number of formed folds and their dimensional size and angular spacing can also be theoretically predicted, as shown in Fig. 2E. Besides, the axial spacing of folds ΔL_f is dependent on the switch angle and initial orientation as indicated in theory (Note S2) and experiments (Fig. S21). Further, when the switch angle does not switch periodically with a sudden change, the woven patterns of film on the substrate will vary significantly. For example, when a transition of 360° is introduced to the transfer, weaving the film on the cylinder substrate will change from one side to the opposite side, as shown in Fig. 2D. Weaving films on a desirable region onto the substrate with controllable spacing could also be achieved by programming the switch angle and transfer directions, as shown in Fig. S22. It should mention that the local folds are crucial for weaving soft films to diverse and complex spatial pattern on partial regions of curved substrate because of their close association with necessary turning of weaving during transfer. Moreover, this fold feature could

potentially be used as step-increase of the r-axis in the 3D manufacturing based on a cylindrical coordinate system $(r-\theta-z)$. In addition, these folds offer an expandable operation space of woven films in response to external stimuli. For example, when an expansion of substrate occurs, the folds could be adjusted with spontaneous releasing to accommodate the mechanical expansion of the substrate, thereby providing mechanical protection to functionality and mechanical integrality of woven spatial structures of films, potentially useful in design of functional 3D structures and devices (40).

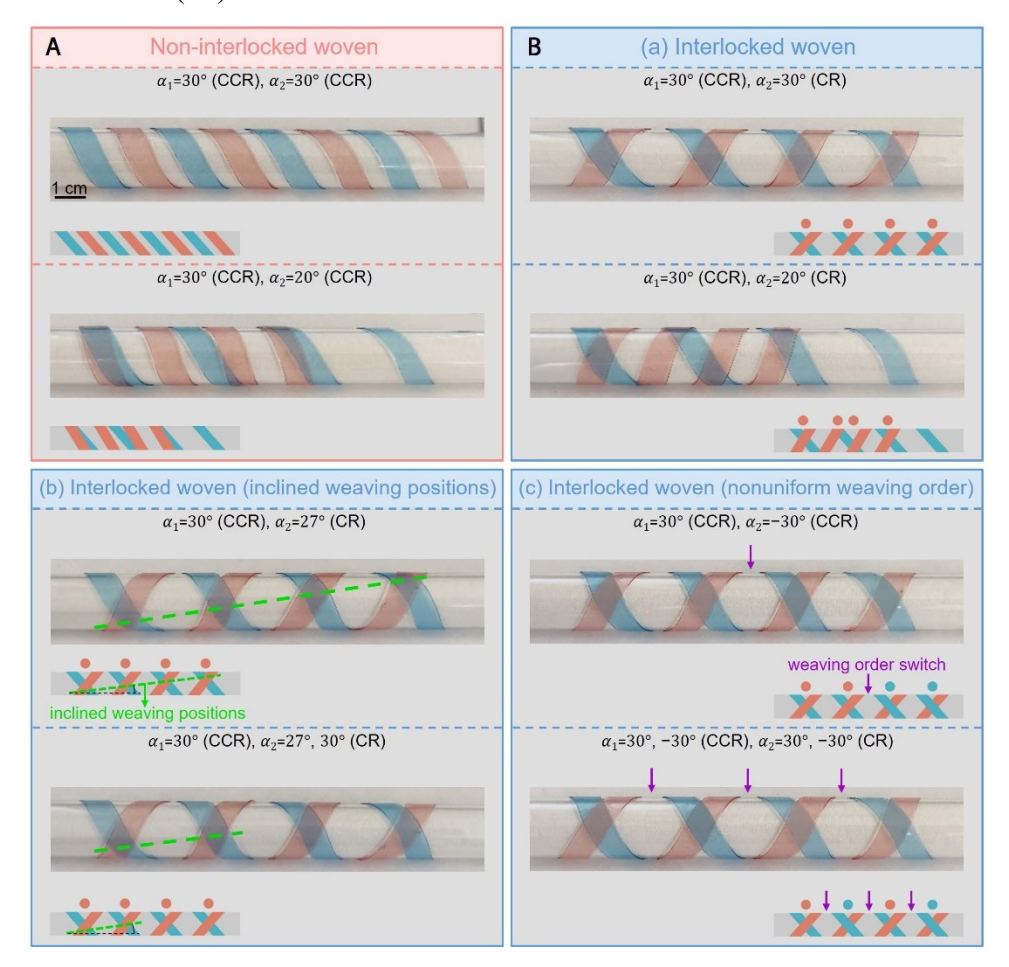


Fig. 3. Weaving spatial structures with two soft films. A, Optical images and schematics (insets) of the non-interlocked woven helical patterns obtained by the transfer of two PDMS films (dyed in blue and red) in the same rolling direction (CCR). The blue film and red film were transferred at same initial orientations $\alpha_1 = \alpha_2 = 30^\circ$ (top) and different initial orientations $\alpha_1 = 30^\circ$ and $\alpha_2 = 20^\circ$ (bottom). B, Optical images and schematics (insets) of the interlocked woven helical patterns weaved by the transfer of two PDMS films in the opposite rolling direction. In the category (a), the blue and the red films were transferred in respective CCR and CR direction at the same initial orientations, generating a symmetrical pattern (top); and when they were transferred at different initial orientations, an asymmetrical pattern is observed (bottom). The category (b) presents the interlocked woven patterns with inclined weaving (intersection)

positions: (top) the films were transferred at $\alpha_1 = 30^\circ$ and $\alpha_2 = 27^\circ$, where the weaving positions fall into the inclined green dash line; (bottom) the orientation α_2 was changed from 27° to 30° during the middle of transfer process, and the resultant weaving positions are only inclined in the first (left) half part of the pattern. The category (c) presents the interlocked woven patterns with non-uniform weaving orders. (top) The films were transferred at $\alpha_1 = 30^\circ$ and $\alpha_2 = -30^\circ$; (bottom) the orientations α_1 and α_2 were changed from 30° to -30° in the transfer process. The red dot in the schematics (insets) denotes the weaving order of red film over blue film and the blue dot denotes the weaving order of blue film over red film. The purple arrows denote the locations where the switch of weaving order occurs.

Weaving structures with multiple soft materials and films

Fig. 3A shows the optical images of two soft films transferred onto the cylinder. The same handedness for both of them is obtained because of the same rolling direction in transfer, leading to non-interlocked woven helical patterns. When their initial orientations (α) on liquid surface vary, the resultant pattern spacing will change, even becomes negative due to generation of the overlaps between them, as shown in Fig. S23A. Particularly, when their initial orientations are different, their handedness remain the same with non-interlocked woven patterns, in good consistency with theoretical predictions in Fig. 1C and Fig. S8. By contrast, when their transfer directions are opposite, they will be woven together with opposite handedness and orientation, forming an interlocked woven pattern, as shown in Fig. 3B. By controlling their initial orientations, different woven patterns on the substrate can be achieved. For example, the same initial orientation leads to a symmetrically woven pattern (Fig. 3B-a), and the weaving (intersection) positions fall into a horizonal line at the center of the pattern. This symmetrically woven pattern is independent of the magnitudes of their initial orientations (Fig. S23A). The asymmetrically woven patterns can be obtained when the initial orientation of both films is different. The weaving positions can be also well controlled along an inclined line as shown in Fig. 3B-b. In addition to the regulation to the weaving patterns, we further conducted the experiments and obtained the interlocked woven patterns with different weaving orders. For example, Fig. 3B-c shows that the weaving order could change with the switch of relative positions between the red and blue films. Besides, both the number and location of the switch could be well controlled. When multiple films are transferred, diverse and complex weaving patterns can be obtained (Fig. S23B).

When local folding deformation is introduced by switching the rolling direction during transfer, the transfer of multiple films onto the cylinder substrate could be not interfered by each

other without any overlap. **Fig. 4A** shows the multiple PDMS films transferred on a single cylinder. Particularly, when the number of transferred films N increases from 2 to 4, the rolling angle θ_f during the transfer of each film needs to decrease from 180° to 90° in order to ensure no overlap among films. Further experiments show that the positions of films on the substrate can also be controlled well (**Fig. S24A**). In addition, by regulating the transition rolling angle during the transfer process, the films can be transferred to multiple positions on the substrate. For instance, with the transition angle 360°, for the transfer of two films (Fig. 4A), the film (dyed in blue) can be transferred from as-planned on the bottom (front view) and left (side view) part of the substrate at the beginning to the top (front view) and right (side view) part of the substrate. Similar results yet rich patterns are obtained when multiple films are transferred, as shown in **Fig. S24B**.

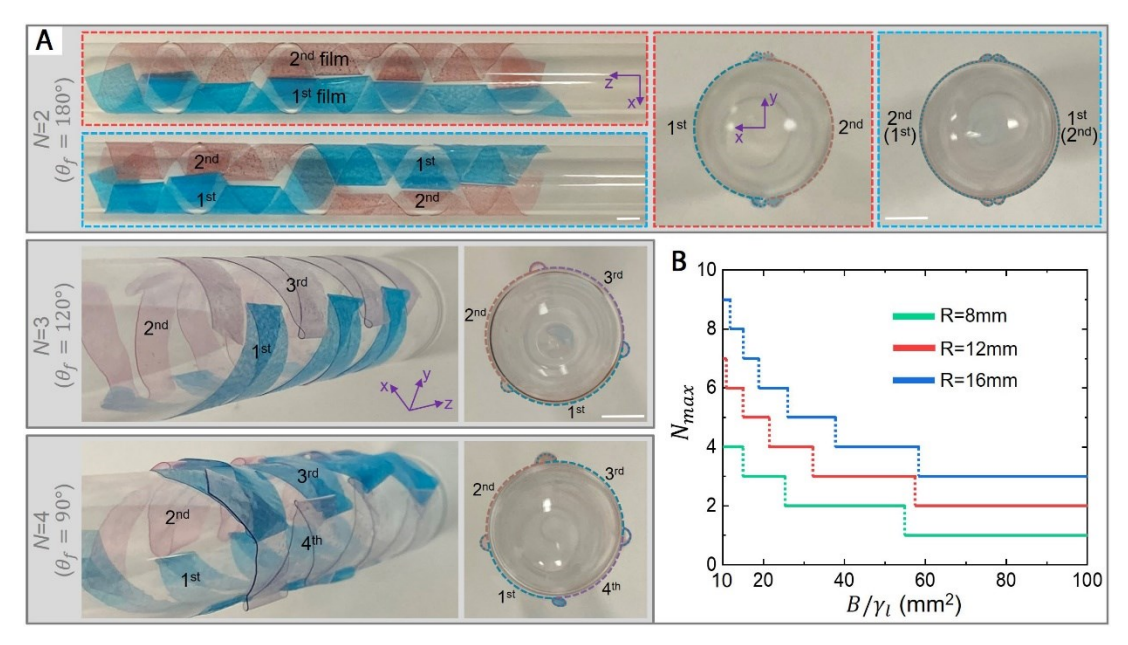


Fig. 4. Transfer and assembly of multiple soft films (materials) without overlap onto a single substrate with the help of local folding deformation. A, Optical images (front, side and oblique views) of multiple PDMS films (dyed in different colors for visualization) transferred on a single glass cylinder, where each film only covers part of the substrate in the angular direction without overlap between them. The number of transferred films N increases from 2 to 4 when the rotation angle θ_f used in the folding and transfer of each film decreases from 180° to 90°. For N=2, the 1st transferred film (blue) is originally only woven on the bottom and left part of substrate (red dash boxed images). With a transition rotation angle at 360° in the middle of transfer, it becomes on the top and right part of substrate (cyan dash boxed images). The scale bar is 5mm. B, Theoretical predictions of the maximum number N_{max} of soft films that can be transferred onto a single substrate without overlap as a function of film stiffness (B) over liquid surface tension (γ_I) for different radius R of cylinder substrates.

When the folding is introduced along with the switch of rolling direction, a minimum rolling angle is required for a successful transfer (Fig. S11B, Note S2). As a result, there is a maximum capacity (N_{max}) that allows to transfer the number of soft films onto substrate without overlap between each other (Note S2). **Fig. 4B** shows its theoretical predictions as a function of normalized film stiffness by liquid surface tension $\frac{B}{\gamma_l}$ for different radius R of cylinder substrate. It suggests that for the thinner films with lower elastic modulus, the larger number of films could be allowed to transfer onto substrates with larger radius.

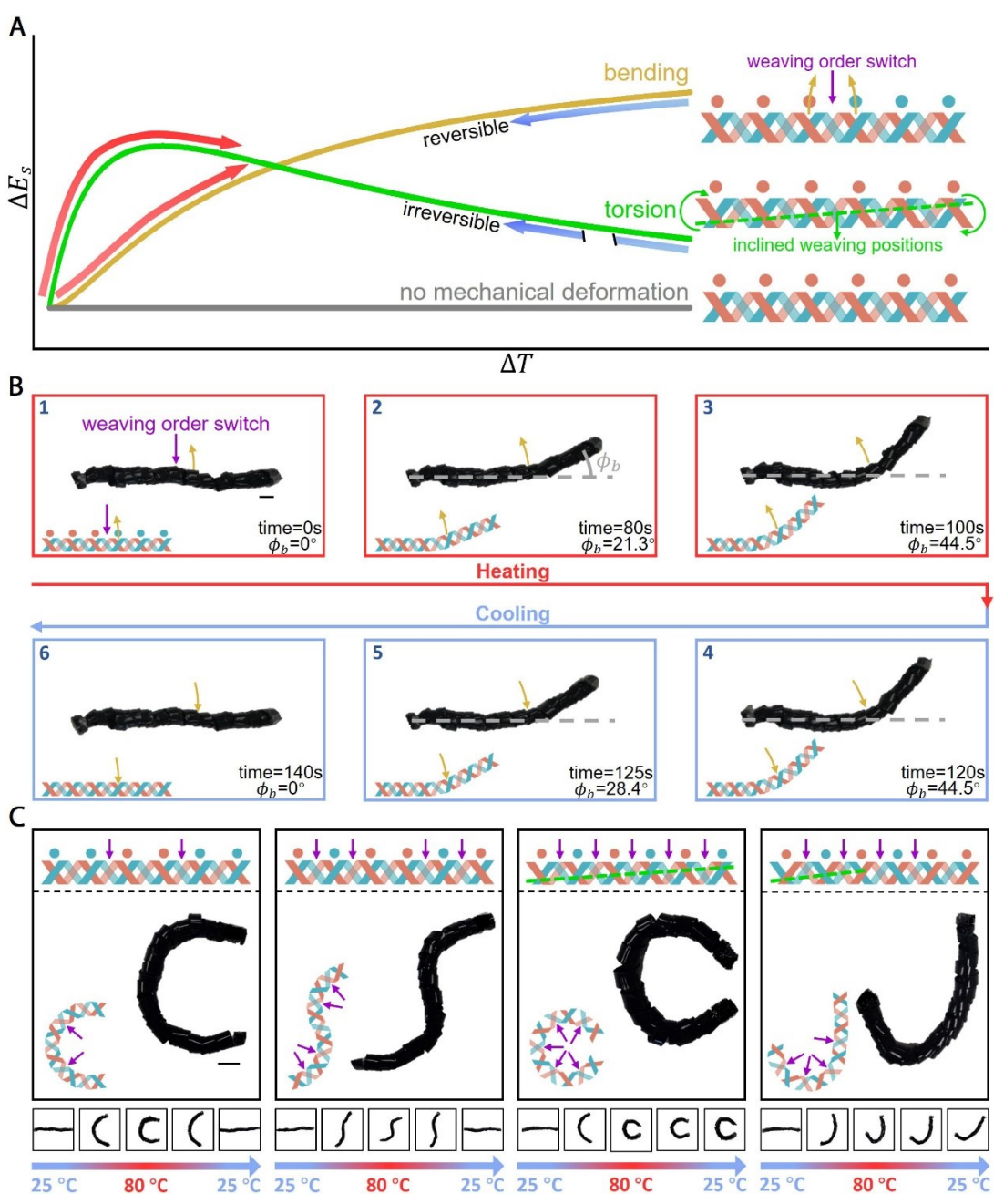


Fig. 5. Application demonstrations of the woven freestanding spatial structure for thermal actuator with multimodal deformation. A, Illustration of energy variation associated with mechanical deformation ΔE_s with temperature change ΔT for realizing basic deformation modes of woven structures (insets). With one switch of weaving order (pointed by the purple arrow), $\Delta T > 0$ leads to $\Delta E_s > 0$, and bending deformation at the position of order switch will occur, where the yellow arrow indicates the bending direction. When the temperature is decreased, ΔE_s will be released, leading to a reversible bending deformation. For the structure with inclined weaving (intersection) positions (highlighted by the green dash line), with $\Delta T > 0$, the resultant ΔE_s first increases and then decreases, leading to an irreversible torsion deformation. The green arrows indicate the torsion direction. No mechanical deformation (i.e., bending and torsion) will happen when the weaving order is uniform with weaving positions at the center. **B**, Optical images of pure bending deformation of freestanding structure during a heating/cooling cycle in the experiment. The structure is bent at the location of weaving order switch (purple arrow), and the bending angle ϕ_b increased in the heating (25°C to 80°C), and decreased back to the original 0 in the cooling (80°C to 25°C). The left end of the structure was fixed in the experiment to highlight the deformation process. Errors of the bending angle ϕ_b measurement are 0.5°. Scale bar is 1cm. C, Programmable deformation modes of woven structures with different designed weaving patterns and orders. The schematics (insets) indicate the weaving patterns of structures and the purple arrows indicate the locations of weaving order switch. The green dash line highlights the inclined weaving positions. Optical images at the bottom show continuous deformation process of structures under one temperature increase/decrease cycle in experiments. Scale bar is 1 cm.

Applications of woven structures for thermal actuator with multi-mode deformation

Once the transferred substrate is removed, spatial structures with programmable weaving orders and patterns suggest potential applications in mimicking living structures and systems in response to an external stimulus. The removal of the substrate can be conducted in liquid with the help of capillary interactions (Fig. S25A, Movie S1). Fig. S25B shows the comparison of both lengths and diameters at different intersection nodes of the structure measured before and after removal of the substrate. The nearly unchanged structure demonstrates a stable removal process without introduction of potential mechanical strain. For the substrate with a complex geometry shape and curvature, the removal could be performed with the aid of etching of sacrificial layer (29). Fig. S25B also proves that the films in the freestanding woven structure can maintain the wrapped shape after the removal of substrate because of the adhesion in the woven overlap between films. Both theory and experiment in good agreement show that the freestanding structures could remain stable, and the stability depends on the balance between the gravity and stiffness (Note S3, Fig. S25C). The spatial woven structure composed of two PDMS/MWCNTs composite films which have fast response to external heat (41) was taken as an

example to demonstrate its function for desirable thermal actuation performance by programming the weaving patterns and orders of films. Consider an heating-induced temperature change ΔT with initial temperature of T_0 , the variation of the mechanical deformation energy ΔE_s of the woven structure is $\Delta E_s = c_1 \left(\frac{\Delta T}{\Delta T + T_0}\right)^2 + c_2 \frac{\Delta T}{\Delta T + T_0}$ (Note S3). Depending on weaving patterns of spatial structures, bending, torsion, and their mixed mode of mechanical deformation can be achieved, as illustrated in **Fig. 5A**. Here, the on-demand weaving patterns can be realized by solely controlling the transfer conditions without the need of touching the properties and geometries of the film materials. For example, when one switch of weaving order is introduced to the spatial structures, bending deformation at the position of order switch will occur, and c_2 0 (Note S3). Therefore, the variation of energy ΔE_s associated with bending deformation increases monotonically with the increasing of temperature ΔT as shown in Fig. 5A. And this also indicates the bending deformation of the structure is reversible when the temperature decreases because the bending deformation will not change the local weaving structure. For the woven structure with inclined weaving (intersection) positions (Fig. 5A, inset), the thermal expansion will lead to a torsion deformation of the structure. The energy associated with the torsion deformation increases with the increasing of temperature, and after the initial energy barrier it will decrease, as shown in Fig. 5A. And this leads to irreversible torsion deformation when the temperature decreases. We should note that when the weaving order in the structures is uniform with weaving positions at the center, no mechanical deformation (i.e., bending and torsion) except for the symmetric expansion is expected (Fig. 5A), and therefore there is no energy change due to mechanical deformation.

Fig. 5B shows a series of experimental snapshots for spatial structures with bending deformation in response to one cycle of temperature increase and decrease (Movie S2), where the left end of the spatial structure was fixed to highlight the bending deformation. The structure is bent at the location of weaving order switch, and the bending angle increases with the increasing of time upon heating. Besides, when the temperature decreased back, the bending angle decreases until back to the original 0 degree, in a good consistency with the theoretical predictions. Similar results are also observed in experiment for torsion deformation of the woven structures, as shown in Fig. S26 and Movie S3. Different from the bending deformation, the local weaving positions were changed by torsion deformation, approaching to the center during

the torsion deformation upon heating. Therefore, torsion deformation remains when the temperature decreases back.

When multiple switches of weaving order are introduced in the woven structures, bending deformation at the corresponding locations are expected upon heating, suggesting the capability of programming modes of deformation. Fig. 5C shows a variety of formed shapes. For example, when there are two switch points of weaving orders located at opposite sides of the structure, the woven structure will be bent at these two points, forming a C-shape pattern. When these two switch points are programmed to the same side, L-shape pattern will be generated (Fig. **S27**). When the switch points increase to four with uniform distance to opposite sides, a S-shape pattern can be obtained. More importantly, because the intersection positions of both films in these woven structures are located at the center, these shapes are all led by pure bending deformation, and will be recovered to the original straight-line shape when the temperature decreases back, as shown in insets in Fig. 5C. By contrast, when a combination of bending and torsion deformation is involved, the programmed shape upon heating could remain. The formation of O-shape pattern involves five periodic switch points of weaving order that are distributed uniformly in the woven structure. Compared with the C-shape pattern, severe bending deformation occurs, indicating an O-shape pattern. Besides, the torsion deformation occurred because of inclined intersection positions (highlight in green dash line) in the woven structure, and as a result, the shape will not recover when the temperature decreases. In addition, when the intersection positions are only inclined at the partial region of the structure, the woven structure could deform to a J-shape pattern upon heating. Upon cooling back to the original temperature, the partial pattern associated with pure bending deformation will recover, but that associated with combined bending and torsion deformation will remain, leading to a check mark-like shape. The achievements of these programmable shapes demonstrate potential applications of manipulating spatial soft structures, capable of mimicking response of living systems to environments and stimuli.

Discussion

In summary, the elasto-capillary transfer technology with a rotational motion mode presented here introduces a weaving and assembly strategy for obtaining spatial structures of soft materials on curvilinear substrates. Fundamental studies of the rolling dynamics at the transfer front among soft material, curved substrate and liquid surface and associated coupling of mechanical deformation of soft materials and fluid dynamics are conducted and establish the foundations for weaving soft materials with solid robustness and reliability. The achievements of woven spatial structures with controllable global weaving chirality, orders and arrangements, and local configurational features validate the feasibility of weaving soft materials into spatial structures by mechanical transfer. As application demonstrations, two thermally conductive films were woven into freestanding spatial structures with on-demand weaving patterns and orders. Their programmable robotic postures including bending, torsion and their combination suggest potentials for broad applications. Guided by theoretical analysis with the established parameter spaces of material selection and system control, integration of this technology with stimuli-responsive materials would help create future manufacturing technologies for fabricating a large diversity of active spatial structures with functionalities adaptive to application environments and could also invoke future exploration of unexpected properties of spatial structures woven by intrinsically planar nanomaterials.

Materials and Methods

Materials

In the fabrication of PDMS film, PDMS (Sylgard 184, Dow Corning Corp.) with 10:1 (otherwise stated) of base polymer to curing agent was first mixed and degassed. Small amount of dye (1.5% by weight) was also added in the mixture for visualization. The mixture was then poured into a Petri dish and placed in 80°C oven for 2 hours to cure. In the fabrication of PDMS/CNT composite film, PDMS with 10:4 base polymer to hexane (n-Hexane, anhydrous, 95%, Sigma-Aldrich) was first mixed and then followed by the addition of multiwalled carbon nanotubes (MWCNTs, 8-15 nm in diameter, 10-50 µm in length, 95%, NanoAmor Inc.). The PDMS-Hexane/MWCNTs mixture was placed in an ultrasonicator for at least 12 hours with 40 kHz to achieve a homogeneous distribution of CNTs. Afterward, the PDMS curing agent was added to the mixture and then degassed before pouring into a glass tank mold. The mold was then delivered to a temperature control chamber to cure at 80°C for 1 hour. The characterization of the mechanical properties of the PDMS and PDMS/CNT films can be found in the reference (26). Both PDMS and PDMS/CNT films were chosen in this work to represent a class of soft and composite materials respectively. Cylindrical glass tubes with different radius were used as substrate in the transfer experiments, and the cylindrical substrates with several other kinds of geometric shapes (such as spherical and cone substrates) were fabricated using a 3D printer (Ultimaker 2+, Ultimaker). To adjust the surface wettability of cylinder substrate, a thin layer of PDMS ($\sim 100 \mu m$ in thickness) was coated onto the surface of substrates. PDMS (10:1 base polymer to curing agent) was mixed with n-Hexane in a 10:4 ratio and degassed. The mixture was then poured onto glass tubes to form uniform layer of PDMS mixture. Coated glass tubes were then cured at 80°C for 2 hours.

Rolling transfer experiments

In the rolling transfer experiments, a clean cylindrical substrate was first submerged in the liquid bath with a depth d and was in contact with one end of the desired film to form the contact line (referred to as the transfer front). The film was placed on the liquid surface with the help of soluble tape and could also be printed directly. The initial orientation between film and substrate is α as illustrated in Fig. 1A. One end of the horizontally oriented cylindrical substrate was fixed co-axially to the shaft of an electric motor. The substrate was driven by the motor to rotate in

either clockwise (CR) or counterclockwise (CCR) direction (35, 42). The rotation speed $\dot{\theta}$ of the substrate could be well adjusted by the motor controller ranging from 1 rpm up to 15 rpm. In each rotation, the overall rotation angle was calculated by $\theta = \dot{\theta}T$, where T was the rotation time. During the rotation of substrate, if the transfer was successful, the film would pass across the transfer front, and was gradually transferred onto the rotating substrate. If the transfer failed, the film could not pass across the transfer front, and would stay on the liquid surface. The rotation of substrate could be paused by the controller of motor at any rotation angle θ during the transfer process. And then when the rotation direction was switched, the film would be folded on the substrate and then transfer would continue in the new direction. However, if the folding failed, the film would slide on the substrate and could not be transferred in the new direction. If the rotation direction was switched back and forth continuously in the transfer process, film with multiple local folds could be transferred onto the substrate. The entire transfer process was recorded by the high-resolution camera placed near the liquid bath. And the image of the film pattern after transfer was also recorded by the high-resolution camera. The pitch Δl and orientation β of the transferred helical pattern were obtained using the image processing software as shown in Fig. 1B. The radius of the fold could also be obtained by the image processing as shown in Fig. S13. After a transfer, the substrate with film could be used as the substrate in the new transfer. In this way, multiple films could be transferred onto the substrate.

Besides, two films can also be transferred together at the same time to achieve woven pattern with desirable weaving orders. Initially, film 1 and 2 are placed at opposite side of the cylindrical substrate. In the first rotation, there can be a weaving order where film 2 (red) is on top of film 1 (blue). And then, in order to change this weaving order, a guidance of film 1 and 2 was required before next rotation, where films were to be pulled into the liquid, underneath the substrate, and out of the liquid to the opposite side of the substrate. The sequence of this guidance of films determines the desired weaving order. If film 2 was pulled first, film 1 will be on top of film 2 instead in the next rotation. And then the woven pattern with a programmable weaving order can be achieved by repeating these processes.

Fabrication of functional spatial woven structure

At first, two PDMS/MWCNTs composite films are used in the transfer considering the good thermal absorption behavior of MWCNTs (41). The diameter of the substrate was chosen as 6

mm to better maintain a stable spatial structure. The formation of spatial structure can be categorized into different types based on the deformation mode (Fig. 5). Assembly of structure with bending mode started with the transfer of film 1 at α_1 =30° in CCR direction, and film 2 at α_2 =30° in CR direction. Besides, the weaving order was changed at least once during the transfer process. Fabrication of structure with torsion mode was different in terms of the initial orientation α . While the initial orientation of film 1, α_1 , remained 30°, α_2 became 27° to introduce the inclined weaving positions between films 1 and 2 in the pattern.

After transfer, the woven spatial structure was made freestanding after taken off from the substrate with the help of capillary interaction (Fig. S25A). Cylindrical substrate with transferred pattern was immersed into the liquid. And then the woven film structure can be easily pulled off from the substrate by hand. Freestanding structure was then carefully picked up from the liquid with a Petri dish and then air-dried for further usage.

Thermal actuation experiment of the spatial woven structures

The woven spatial structure with on-demand weaving patterns and orders was first gently placed on the surface of the water bath, and then both delivered to a temperature control chamber. Replacing conventional hard, solid substrate with water substrate helps reduce the friction force generated between films and solid substrate during actuation. One end of the structure was clamped for better imaging. Depends on different weaving patterns of structure, pure bending deformation, pure torsion deformation, and their combination in the structures can be realized by increasing the temperature in the chamber. After that, the temperature was decreased back to the original. Video recording of the deformation and recovering processes of the structures was also accomplished in the experiment (Movies S2 and S3).

References

- 1. T. Xu, J. Zhang, M. Salehizadeh, O. Onaizah, E. Diller, Millimeter-scale flexible robots with programmable three-dimensional magnetization and motions. *Science Robotics* **4**, eaav4494 (2019).
- 2. W. Hu, G. Z. Lum, M. Mastrangeli, M. Sitti, Small-scale soft-bodied robot with multimodal locomotion. *Nature* **554**, 81-85 (2018).
- 3. J. H. Lee, C. Y. Koh, J. P. Singer, S. J. Jeon, M. Maldovan, O. Stein, E. L. Thomas, 25th anniversary article: Ordered polymer structures for the engineering of photons and phonons. *Advanced Materials* **26**, 532-569 (2014).
- 4. C. Choi, M. K. Choi, S. Liu, M. S. Kim, O. K. Park, C. Im, J. Kim, X. Qin, G. J. Lee, K. W. Cho, Human eye-inspired soft optoelectronic device using high-density MoS2-graphene curved image sensor array. *Nature communications* 8, 1-11 (2017).
- 5. M. Boncheva, S. A. Andreev, L. Mahadevan, A. Winkleman, D. R. Reichman, M. G. Prentiss, S. Whitesides, G. M. Whitesides, Magnetic self-assembly of three-dimensional surfaces from planar sheets. *Proceedings of the National Academy of Sciences* **102**, 3924-3929 (2005).
- 6. K. Sim, S. Chen, Z. Li, Z. Rao, J. Liu, Y. Lu, S. Jang, F. Ershad, J. Chen, J. Xiao, Three-dimensional curvy electronics created using conformal additive stamp printing. *Nature Electronics* **2**, 471-479 (2019).
- 7. J. Cui, T.-Y. Huang, Z. Luo, P. Testa, H. Gu, X.-Z. Chen, B. J. Nelson, L. J. Heyderman, Nanomagnetic encoding of shape-morphing micromachines. *Nature* **575**, 164-168 (2019).
- 8. S. Fusco, M. S. Sakar, S. Kennedy, C. Peters, R. Bottani, F. Starsich, A. Mao, G. A. Sotiriou, S. Pané, S. E. Pratsinis, An integrated microrobotic platform for on-demand, targeted therapeutic interventions. *Advanced Materials* **26**, 952-957 (2014).
- 9. H. Luan, Q. Zhang, T.-L. Liu, X. Wang, S. Zhao, H. Wang, S. Yao, Y. Xue, J. W. Kwak, W. Bai, Complex 3D microfluidic architectures formed by mechanically guided compressive buckling. *Science advances* 7, eabj3686 (2021).
- 10. X. Liu, H. Yuk, S. Lin, G. A. Parada, T. C. Tang, E. Tham, C. de la Fuente-Nunez, T. K. Lu, X. Zhao, 3D printing of living responsive materials and devices. *Advanced Materials* **30**, 1704821 (2018).
- 11. X. Zhao, J. Kim, C. A. Cezar, N. Huebsch, K. Lee, K. Bouhadir, D. J. Mooney, Active scaffolds for on-demand drug and cell delivery. *Proceedings of the National Academy of Sciences* **108**, 67-72 (2011).
- 12. M. Sitti, Miniature soft robots—road to the clinic. *Nature Reviews Materials* **3**, 74-75 (2018).
- 13. X. Wang, M. Jiang, Z. Zhou, J. Gou, D. Hui, 3D printing of polymer matrix composites: A review and prospective. *Composites Part B: Engineering* **110**, 442-458 (2017).
- 14. C. B. Dayan, S. Chun, N. Krishna-Subbaiah, D. M. Drotlef, M. B. Akolpoglu, M. Sitti, 3D Printing of Elastomeric Bioinspired Complex Adhesive Microstructures. *Advanced Materials* **33**, 2103826 (2021).
- 15. A. Kotikian, R. L. Truby, J. W. Boley, T. J. White, J. A. Lewis, 3D printing of liquid crystal elastomeric actuators with spatially programed nematic order. *Advanced materials* **30**, 1706164 (2018).
- 16. Z. Wang, Z. Wang, Y. Zheng, Q. He, Y. Wang, S. Cai, Three-dimensional printing of functionally graded liquid crystal elastomer. *Science advances* **6**, eabc0034 (2020).

- 17. M. K. Blees, A. W. Barnard, P. A. Rose, S. P. Roberts, K. L. McGill, P. Y. Huang, A. R. Ruyack, J. W. Kevek, B. Kobrin, D. A. Muller, Graphene kirigami. *Nature* **524**, 204-207 (2015).
- 18. Q. Zhao, W. Zou, Y. Luo, T. Xie, Shape memory polymer network with thermally distinct elasticity and plasticity. *Science advances* **2**, e1501297 (2016).
- 19. M. Z. Miskin, K. J. Dorsey, B. Bircan, Y. Han, D. A. Muller, P. L. McEuen, I. Cohen, Graphene-based bimorphs for micron-sized, autonomous origami machines. *Proceedings of the National Academy of Sciences* **115**, 466-470 (2018).
- 20. H. Fu, K. Nan, W. Bai, W. Huang, K. Bai, L. Lu, C. Zhou, Y. Liu, F. Liu, J. Wang, Morphable 3D mesostructures and microelectronic devices by multistable buckling mechanics. *Nature materials* 17, 268-276 (2018).
- 21. Z. Yan, F. Zhang, J. Wang, F. Liu, X. Guo, K. Nan, Q. Lin, M. Gao, D. Xiao, Y. Shi, Controlled mechanical buckling for origami-inspired construction of 3D microstructures in advanced materials. *Advanced functional materials* **26**, 2629-2639 (2016).
- 22. J. Shim, C. Perdigou, E. R. Chen, K. Bertoldi, P. M. Reis, Buckling-induced encapsulation of structured elastic shells under pressure. *Proceedings of the National Academy of Sciences* **109**, 5978-5983 (2012).
- 23. Y. Li, H. Yu, K. Yu, X. Guo, X. Wang, Reconfigurable Three-Dimensional Mesotructures of Spatially Programmed Liquid Crystal Elastomers and Their Ferromagnetic Composites. *Advanced Functional Materials* **31**, 2100338 (2021).
- 24. W. Lee, Y. Liu, Y. Lee, B. K. Sharma, S. M. Shinde, S. D. Kim, K. Nan, Z. Yan, M. Han, Y. Huang, Two-dimensional materials in functional three-dimensional architectures with applications in photodetection and imaging. *Nature communications* **9**, 1-9 (2018).
- 25. S. Xu, Z. Yan, K.-I. Jang, W. Huang, H. Fu, J. Kim, Z. Wei, M. Flavin, J. McCracken, R. Wang, A. Badea, Y. Liu, D. Xiao, G. Zhou, J. Lee, H. U. Chung, H. Cheng, W. Ren, A. Banks, X. Li, U. Paik, R. G. Nuzzo, Y. Huang, Y. Zhang, J. A. Rogers, Assembly of micro/nanomaterials into complex, three-dimensional architectures by compressive buckling. *Science* 347, 154-159 (2015).
- 26. Y. Zhang, M. Yin, Y. Baek, K. Lee, G. Zangari, L. Cai, B. Xu, Capillary transfer of soft films. *Proceedings of the National Academy of Sciences* **117**, 5210-5216 (2020).
- 27. A. Okmi, X. Xiao, Y. Zhang, R. He, O. Olunloyo, S. B. Harris, T. Jabegu, N. Li, D. Maraba, Y. Sherif, Discovery of Graphene-Water Membrane Structure: Toward High-Quality Graphene Process. *Advanced Science*, 2201336 (2022).
- 28. J. K. Park, Y. Zhang, B. Xu, S. Kim, Pattern transfer of large-scale thin membranes with controllable self-delamination interface for integrated functional systems. *Nature communications* **12**, 1-10 (2021).
- 29. D. S. Wie, Y. Zhang, M. K. Kim, B. Kim, S. Park, Y.-J. Kim, P. P. Irazoqui, X. Zheng, B. Xu, C. H. Lee, Wafer-recyclable, environment-friendly transfer printing for large-scale thin-film nanoelectronics. *Proceedings of the National Academy of Sciences* 115, E7236-E7244 (2018).
- 30. J. Yan, A. Moreau, S. Khodaparast, A. Perazzo, J. Feng, C. Fei, S. Mao, S. Mukherjee, A. Košmrlj, N. S. Wingreen, Bacterial biofilm material properties enable removal and transfer by capillary peeling. *Advanced Materials* **30**, 1804153 (2018).
- 31. S. W. Song, S. Lee, J. K. Choe, N.-H. Kim, J. Kang, A. C. Lee, Y. Choi, A. Choi, Y. Jeong, W. Lee, J.-Y. Kim, S. Kwon, J. Kim, Direct 2D-to-3D transformation of pen drawings. *Science Advances* 7, eabf3804 (2021).

- 32. F. Zhang, D. Li, C. Wang, Z. Liu, M. Yang, Z. Cui, J. Yi, M. Wang, Y. Jiang, Z. Lv, Shape morphing of plastic films. *Nature communications* **13**, 1-13 (2022).
- 33. C. Py, P. Reverdy, L. Doppler, J. Bico, B. Roman, C. N. Baroud, Capillary origami: spontaneous wrapping of a droplet with an elastic sheet. *Physical review letters* **98**, 156103 (2007).
- 34. J. Luo, H. D. Jang, T. Sun, L. Xiao, Z. He, A. P. Katsoulidis, M. G. Kanatzidis, J. M. Gibson, J. Huang, Compression and aggregation-resistant particles of crumpled soft sheets. *ACS nano* 5, 8943-8949 (2011).
- 35. F. Henrich, D. Fell, D. Truszkowska, M. Weirich, M. Anyfantakis, T.-H. Nguyen, M. Wagner, G. K. Auernhammer, H.-J. Butt, Influence of surfactants in forced dynamic dewetting. *Soft Matter* **12**, 7782-7791 (2016).
- 36. S. Liu, J. He, Y. Rao, Z. Dai, H. Ye, J. C. Tanir, Y. Li, N. Lu, Conformability of flexible sheets on spherical surfaces. *Science Advances* **9**, eadf2709 (2023).
- 37. Q. Liu, J. Huang, B. Xu, Evaporation-driven crumpling and assembling of two-dimensional (2D) materials: A rotational spring—mechanical slider model. *Journal of the Mechanics and Physics of Solids* **133**, 103722 (2019).
- 38. J. Liu, S. Jiang, W. Xiong, C. Zhu, K. Li, Y. Huang, Self-Healing Kirigami Assembly Strategy for Conformal Electronics. *Advanced Functional Materials* **32**, 2109214 (2022).
- 39. Y.-K. Lee, Z. Xi, Y.-J. Lee, Y.-H. Kim, Y. Hao, H. Choi, M.-G. Lee, Y.-C. Joo, C. Kim, J.-M. Lien, Computational wrapping: A universal method to wrap 3D-curved surfaces with nonstretchable materials for conformal devices. *Science advances* 6, eaax6212 (2020).
- 40. Y. Park, C. K. Franz, H. Ryu, H. Luan, K. Y. Cotton, J. U. Kim, T. S. Chung, S. Zhao, A. Vazquez-Guardado, D. S. Yang, Three-dimensional, multifunctional neural interfaces for cortical spheroids and engineered assembloids. *Science advances* 7, eabf9153 (2021).
- 41. L. Chen, C. Liu, K. Liu, C. Meng, C. Hu, J. Wang, S. Fan, High-performance, low-voltage, and easy-operable bending actuator based on aligned carbon nanotube/polymer composites. *ACS nano* 5, 1588-1593 (2011).
- 42. B. A. Puthenveettil, V. K. Senthilkumar, E. Hopfinger, Motion of drops on inclined surfaces in the inertial regime. *Journal of Fluid Mechanics* **726**, 26-61 (2013).

Acknowledgments:

Funding: This work is supported by NSF CMMI-1728149, NSF-CMMI-1928788 and Virginia Microelectronics Consortium (VMEC).

Author contributions: B. X. conceived and designed the project, Y. Z. developed theory models, Y.Z. and M. Y. performed experiments. All authors discussed the results and wrote the manuscript.

Competing interests: The authors declare that they have no competing interests.

Data and materials availability: All data are available in the main text or the supplementary materials.

Supplementary Materials

Figs. S1 to S27

Movies S1 to S3

Notes S1 to S3